Journal of Sound and Vibration (1997) **203**(3), 473–493

DISTRIBUTED SENSOR/ACTUATOR DESIGN FOR PLATES: SPATIAL SHAPE AND SHADING AS DESIGN PARAMETERS

J. M. SULLIVAN

USAF Phillips Laboratory PL/VTV, 3550 *Aberdeen Ave. SE*, *Kirtland AFB*, *NM* 87117-5776, *U.S.A.*

AND

J. E. HUBBARD, JR. AND S. E. BURKE

Centre for Photonics Research, *Boston University*, 143 *Bay State Rd.*, *Boston*, *MA* 02215, *U.S.A.*

(*Received* 28 *February* 1996, *and in final form* 13 *November* 1996)

This paper will discuss two-dimensional distributed transducer shape and shading and their implications for the active control of plates. Two-dimensional transducer shaping is shown to be a useful design tool for the control problem. In addition, transducer shaping can be combined with gain-weighting to provide close approximation of continuously shaded transducer distributions. An optimization method is described which can be used to fit the approximation to a continuous distribution. The analysis is applied to two examples of transducers used to control a rectangular, simply-supported plate. The first relies on shaping alone and is shown to spatially filter out the even-even modes. The second was developed using the optimization technique and is shown to provide "all-mode" controllability and observability.

1. INTRODUCTION

Several researchers have examined the use of distributed transducers for the active control of two-dimensional structures [1–3]. The possible applications include both vibration suppression and acoustic radiation attenuation. The primary advantage of distributed transducers is that they can be shaded by varying their gain over their spatial extent. Through the application of shaded transducers, the transducer-augmented forward-loop transfer function can be altered so as to achieve desired temporal and spatial performance goals [4]. This paper describes methods for achieving two-dimensional transducer shading using *two-dimensionally* shaped transducers.

Prior work by the authors [5] has included the development of an analytical method for modelling two-dimensionally shaped transducers. The method will be used in this paper to aid in the design of two-dimensional transducer distributions for the active control of plates. Because the method is analytical, much insight is obtained into the physics of the interaction between the shaped transducer and mode shapes in a plate.

Shaped sensors and actuators have previously been utilized for mode targeting, loop shaping, and for all-mode sensing and control for beams [6–12]. Because these transducers were applied to beams, no transverse modes of vibration were present, and the shapes were good approximations of continuous, one-dimensional shading. Burke and Hubbard [6] and Miller and Hubbard [7] developed a design methodology for shaded transducers to

0022–460X/97/230473 + 21 $25.00/0/sv960877

accomplish all-mode sensing and control for beams with arbitrary combinations of boundary conditions. They verified these techniques using shaped PVDF actuators and sensors [7, 8]. Lee and Moon [9] and Lee *et al*. [10, 11] demonstrated modal damping in beams using shaped PVDF transducers. Miller *et al*. [12] reviewed the use of shaped PVDF sensors used to create desired spatial filtering properties for beams.

Clark and Fuller [3, 13], Clark *et al*. [14], and Burke and Clark [15] investigated shaped sensors for sensing acoustically significant modes in plates. However, these were also shapes which were designed to be good approximations to continuous one-dimensional shading. Even though these shaped transducers were applied to plates, their width was small in comparison with the smallest transverse wavelength present in the plate's dynamic response. However, errors in the placement of these sensors can lead to coupling with undesired modes in experimental implementations [15].

The location and size of unshaded rectangular actuators have been studied by Dimitriadis *et al*. [16] for structural acoustic control of plates. Shaping a distributed transducer into a non-rectangular shape is actually a form of two-dimensional shading: the gain is varied discontinuously over two-dimensions. Transducer shaping alone can provide useful modal coupling for plates. Burke and Hubbard [2] have extended the concept of continuous shading for beams to plates. Their work theoretically demonstrated that all-mode sensing and control could be achieved for plates through the use of continuous, two-dimensionally shaded transducers. While one-dimensional shading for beams and structural beam components can be easily approximated using shaped distributed transducers, the practical realization of two-dimensional shading in distributed transducers for plates is more difficult. A potential method outlined in this paper uses a superposition of gain-weighted, shaped transducers.

In this paper, two-dimensional transducer shading and its implications for the active control of thin plates are discussed. Candidate methods of producing shaded transducers are also reviewed. Two-dimensional transducer shaping is presented as a useful design tool for the control problem. A method is described for approximating continuously shaded transducer distributions with a combination of transducer shaping and spatial gain-weighting. Wavenumber transforms are also used to evaluate controllability and observability. An optimization method used to fit the shaped transducer approximations to a continuous transducer distribution over a specified number of modal coefficients is then detailed. The analysis is applied to two specific examples. Both consider rectangular plates with simply-supported boundary conditions. The analysis of simply-supported plates provides insight for many classes of panel vibration problems [17].

One example utilizes two-dimensional transducer shaping and mode targeting alone to establish controllability and observability over all but the even–even modes in a simply-supported plate. This transducer distribution is a very practical solution for the acoustic radiation attenuation problem. The second distribution is a superposition of

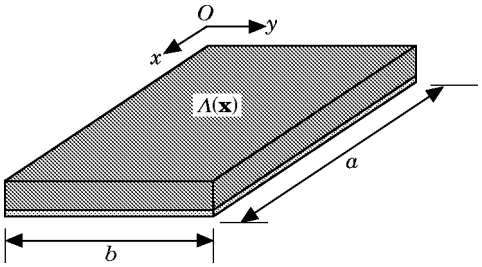

Figure 1. Uniform transducer distribution.

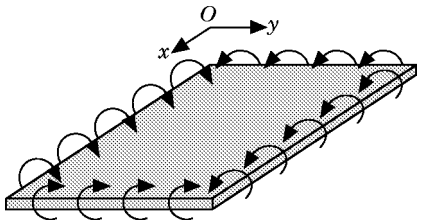

Figure 2. Resultant control input/sensed output for uniform transducer distribution.

gain-weighted, shaped transducer sections, which provide a good approximation to a continuous two-dimensionally shaded transducer distribution. This distribution provides "all-mode" controllability and observability over a large bandwidth and is therefore useful for global vibration suppression.

2. ANALYSIS

2.1. MOTIVATION FOR SHADING

To understand the utility of two-dimensional shaded transducers for plates, one must first examine the limits that uniformly-weighted distributed transducers place on controllability and observability for plates. The following discussion is a review of the plate control study by Burke and Hubbard [2]. Consider the transducer distribution, $\Lambda(x, y)$, laminated to a rectangular, simply supported plate shown in Figure 1. The transducer is assumed to be an induced-strain type such as piezopolymer film (PVDF) or a piezoceramic crystal (PZT). This distribution is even-symmetric about both centerlines, $x = a/2$ and $y = b/2$. If the material axes of this transducer are coincident with the axes of the plate, then the resultant control input/sensed output for the plate is shown in Figure 2. Distributed doublet functions are obtained along the entire boundary. If the transducer were used as an actuator, these would correspond to uniform distributed bending moments. If the transducer were used as a sensor, it would be able to sense uniform angular displacement along the boundary.

The inherent even–even symmetry of the unshaded distribution limits the efficacy of this transducer when used as either a sensor or an actuator. Consider the 2–1 mode and 2–2 modes of a simply-supported plate as shown in Figure 3 and Figure 4, respectively. Whenever the angular velocity distributions along opposing sides of the plate are equal, the unshaded transducer cannot do work or sense any motion in the direction normal to those sides. This occurs along sides $x = 0$ and $x = a$ in Figure 3. Whenever the integrated angular velocity distributions along opposing sides of the plate are zero, the same result will hold. This is true for sides $y = 0$ and $y = b$ in Figure 3 and for all sides in Figure 4. Thus, this unshaded rectangular distribution will not be able to control or sense modes

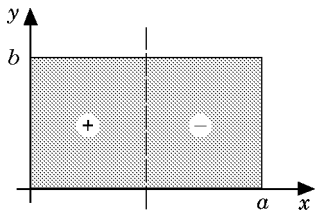

Figure 3. 2,1 mode of simply-supported plate (— —, nodal line).

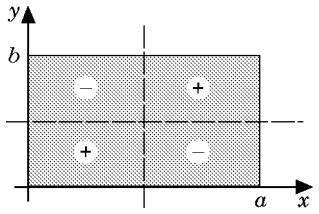

Figure 4. 2,2 mode of simply-supported plate (— —, nodal line).

with odd–even, even–odd, or even–even symmetry. If this transducer were reduced in size but remained centred on the plate, it would still lack both controllability and observability for these modes.

By spatially varying the input/output characteristics of the transducer, i.e., by *shading* it, this symmetry problem can be resolved [2]. Shading the transducer in two dimensions gives it the different types of symmetry required to sense and control all modes of the simply supported plate. An example of a shaded transducer distribution is shown in Figure 5. Note that the amplitude of the transducer distribution varies continuously over the surface of the plate. The transducer is shaded over two dimensions such that the gain is at a maximum, $\Lambda_{\max}$, at one corner, $(x, y) = (0, 0)$, but decreases linearly to zero in both the x and y directions. Thus, this transducer distribution has both even and odd symmetry about each of the centre lines, $x = a/2$ and $y = b/2$.

The resultant control input/sensed output for the simply-supported plate is shown in Figure 6. In contrast to the uniform transducer distribution, the induced moments/sensed angular velocity distributions are now only present on two adjacent sides of the plate, $x = 0$ and $y = 0$, and are weighted to decrease linearly from a maximum at the point (0, 0) to zero at the points $(a, 0)$ and $(0, b)$. This distribution can control and sense the modes that the uniform distribution could not. Because the moments occur only along $x = 0$ and $y = 0$, the cancellation due to equal angular velocity distributions along opposing sides of the plate is avoided. In addition, due to the weighting of the moments along each side, it is possible to sense modes where the integrated angular velocity along a side of the plate is zero. Thus, all of the modes which could be present in a simply-supported plate can be controlled and sensed using the shaded distribution.

The above discussion used a simply-supported plate and a specific two-dimensional transducer shading as an example. However, two-dimensional shaded transducer distributions can be designed so as to exhibit all-mode sensing and control in plates with arbitrary boundary conditions [2]. When combined with a feedback controller such as velocity feedback, this is very beneficial for the problem of global vibration suppression

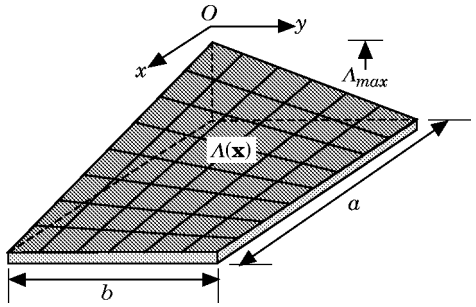

Figure 5. Continuously shaded transducer distribution.

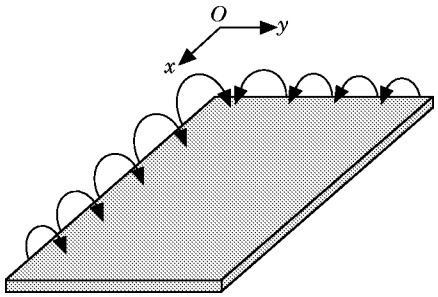

Figure 6. Resultant control input/sensed output for continuously shaded transducer distribution.

in plates. To enhance stability robustness and increase performance, the shading can also be tailored so as to couple evenly into modes within a certain bandwidth and then roll-off for higher frequency modes. Thus, the system can be compensated spatially, through tailoring of the modal coefficients, to more effectively deal with temporal phase lag problems associated with real hardware such as analog filters and power supplies. That is the real benefit of shading: to be able to change the spatial filtering characteristics of an elastic system to improve both stability and performance [4].

Another benefit of two-dimensional shading is in the design of transducers to control and sense only acoustically significant modes in panels. Sensing of acoustically significant modes in simply-supported plates has been studied previously using one-dimensionally shaded sensors [3, 13–15], but with two-dimensional shadings, the work can be expanded to develop both actuator and sensor distributions for plates with other boundary conditions. In these cases, the spatial filtering properties of plates can be changed so as to move energy from acoustically significant modes into those modes which are inefficient sound radiators.

2.2. METHODS FOR SHADING TWO-DIMENSIONAL PIEZOELECTRIC TRANSDUCERS

The previous section reviewed the definition of two-dimensional shading and considered the benefits of shading from a physical standpoint. In the following discussion, the concepts will be formalized by examining the means for implementing shading using piezopolymer film (PVDF). This material is quite useful for producing two-dimensional shaded transducer distributions. It is tough and flexible, and can be laminated over large surface areas. The electrode plating of the material can be manufactured with unique shapes, or the material can be cut to the desired shape.

The differential operator describing the spatial dynamics of piezopolymer film (PVDF), with the possibility of a skew angle, θ, between the transducer and structure axes, is given by Lee and Moon [1]:

$$L[\Lambda(x, y)] = e_{31}^0 \frac{\partial^2 \Lambda(x, y)}{\partial x^2} + e_{32}^0 \frac{\partial^2 \Lambda(x, y)}{\partial y^2} + e_{36}^0 \frac{\partial^2 \Lambda(x, y)}{\partial x \partial y}, \tag{1}$$

with

$$\begin{bmatrix} e_{31}^0 \\ e_{32}^0 \\ e_{36}^0 \end{bmatrix} = \begin{bmatrix} \cos^2\theta & \sin^2\theta & -2\cos\theta\sin\theta \\ \sin^2\theta & \cos^2\theta & 2\cos\theta\sin\theta \\ \cos\theta\sin\theta & -\cos\theta\sin\theta & \cos^2\theta - \sin^2\theta \end{bmatrix}$$

$$\times \begin{bmatrix} Y_p/(1-v_p^2) & v_p Y_p/(1-v_p^2) & 0 \\ v_p Y_p/(1-v_p^2) & Y_p/(1-v_p^2) & 0 \\ 0 & 0 & Y_p/[2(1+v_p)] \end{bmatrix} \begin{bmatrix} d_{3'1'}^0 \\ d_{3'2'}^0 \\ 0 \end{bmatrix}, \tag{2}$$

where e_{31}^0, e_{32}^0, e_{36}^0 represent the piezoelastic stress/charge constants with respect to the structure axes; $d_{3'1'}^0$, $d_{3'2'}^0$ are the piezoelectric strain/charge constants with respect to the PVDF material axes; and Y_p, v_p are the Young's modulus and Poisson ratio, respectively, of PVDF.

Both the actuator and sensor equations for PVDF laminated to a thin plate are based upon this differential operator. The skew angle, θ, can be varied to change the values of the stress/charge constants. These constants weigh each partial differential term in the operator but cannot change the characteristics of the resultant terms of the operator. The characteristics of the resultant terms of the operator are affected only by the distribution function, $\Lambda(x, y)$, that is included under partial differentiation.

The spatial distribution of the transducer, $\Lambda(x, y)$, can be separated into two functions:

$$\Lambda(x, y) = F(x, y)P_0(x, y), \tag{3}$$

where $F(x, y)$ describes the shape of the PVDF and is defined as being equal to one within the transducer boundary and zero otherwise. $P_0(x, y)$ is the polarization profile of the PVDF and is assumed to be unity for film which has not been repolarized after manufacture.

One may vary the piezopolymer gain over two-dimensions by spatially varying either $\Lambda(x, y)$ or the electric field applied to the PVDF. It is possible to spatially weight the electric field used to pole the material during manufacture. This would affect the piezoelectric properties of the material, represented in the operator equation by the strain/charge constants. It is also possible to affect the polarization after manufacture by repoling (or depoling) the material with another strong electric field. Lee and Moon have accounted for this process with the $P_0(x, y)$ function which represents the polarization profile of the film. Hence, the material would arrive from the factory with certain values for the strain/charge constants which were constant over the extent of the film. The $P_0(x, y)$ would be equal to one for all (x, y). By applying a strong electric field to change the polarization profile, the overall effect in the operator would be to scale the piezoelectric properties of the film with respect to the factory values of the strain/charge constants.

Thickness variations in either the plate or the film can also cause shading. Thickness variation in the film will change the applied electric field because the electric field is equal to the voltage applied to the film electrodes divided by the film thickness. Thickness variation in the bonding layer, or in an added shim, will change the moment arm of the transducer relative to the center plane of the plate.

Another way to change the spatial distribution of the film would be to change its electrode shape $F(x, y)$. Non-rectangular shapes can be used to achieve desired shading effects in much the same way that shaped electrodes have been used for beam problems. However, shaping the film does not continuously change its gain over space. The film will have unit magnitude gain within the shape boundary and zero magnitude outside of the boundary.

During actual use, one can vary the electric field applied to the PVDF. One way to do this is to vary the voltage applied to the electrodes over space by gain-weighting transducer subsections. This technique, combined with varying the transducer's electrode shape, can be used to approximate a two-dimensional shading. Of the various techniques described in this section, transducer shaping and gain-weighting are the most practical for implementing two-dimensional shading. These techniques will be described in more detail

in the next section and sample distributions will be presented which possess useful spatial filtering properties.

2.3. MATHEMATICAL MODELLING: CALCULATION OF MODAL COEFFICIENTS FOR PLATES

To evaluate possible methods of shading the distribution of PVDF film, one can study the resultant effects of shading on modes of vibration in plates. Consider the free response of a Bernoulli–Euler plate. The response can be expressed as a sum of orthogonal modes separable in space and time:

$$w(t, \mathbf{x}) = \sum_{n=1}^{\infty} w_n(t)\varphi_n(\mathbf{x}) \tag{4}$$

where n is the mode number, $w_n(t)$ is a harmonic function of time with natural frequency, β_n, and φ_n is the modal shape.

Burke and Hubbard [2] used Lyapunov functionals to assess the impact of shading on controllability and observability for plates, but similar results can be derived by examination of the actuator and sensor modal coefficients. The use of modal coefficients is better suited for the study of complex two-dimensional transducer distributions because information about the plate modal symmetry is taken into account in their calculation. The nth modal coefficient for a two dimensional transducer applied to a plate of domain, D, is given by [2, 18]

$$b_n = c_n = \int_D \varphi_n(\mathbf{x}) L[\Lambda(\mathbf{x})]\, \mathrm{d}\mathbf{x}. \tag{5}$$

The nth actuator modal coefficient for the transducer, b_n, shows how the transducer, when used as an actuator, couples into individual modes of vibration. Conversely, the sensor modal coefficient, c_n, shows how well the transducer, when used as a sensor, senses individual modes. The modal coefficients characterize the impact of shading on plates and can serve as a measure for shading approximations. Note that the value of this modal coefficient depends upon the plate mode shape $\varphi_n(\mathbf{x})$, the transducer spatial distribution $\Lambda(x, y)$, and the differential operator describing the transducer's spatial dynamics, $L[.]$. For illustrative purposes, assume that the plate under consideration is simply-supported along all sides. This allows the mode shapes to be separated into one-dimensional sinusoids in x and y,

$$\varphi_n(\mathbf{x}) = \varphi_r(x)\varphi_q(y) = A_{rq} \sin(r\pi x/a) \sin(q\pi y/b), \tag{6}$$

where A_{rq} is determined by normalization of the mode shapes. If a mass or stiffness normalization is used, then this value is a constant for all modes and it will therefore be neglected in the rest of the analysis. These mode shapes will be used in the following analysis to calculate modal coefficients for a variety of transducer spatial distributions.

In previous work by the authors [5], arbitrary two-dimensional transducer distributions were modelled using two-dimensional step functions with composite functions included in the arguments. The theory needed to calculate the PVDF differential operator acting on these distributions was also developed. The arbitrary transducer shape shown in Figure 7 can be represented concisely by

$$\Lambda(x, y) = (\langle x - x_2\rangle^0 - \langle x - x_1\rangle^0)(\langle y - f_2(x)\rangle^0 - \langle y - f_1(x)\rangle^0). \tag{7}$$

Macauley notation [19] is used to represent the step functions. For example, $\langle x - a\rangle^0$ represents a step function $h(x - a)$, which begins at $x = a$. The derivative with respect to

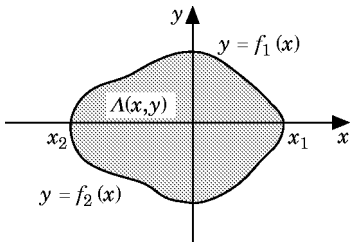

Figure 7. Arbitrary transducer shape in rectangular co-ordinates.

x of this function is given by $\langle x-a\rangle^{-1}$. This is the delta function $\delta(x-a)$, at $x=a$. The partial derivatives needed to calculate the PVDF differential operator acting on the distribution are given by

$$\frac{\partial \Lambda(x,y)}{\partial x} = (\langle x-x_2\rangle^{-1} - \langle x-x_1\rangle^{-1})(\langle y-f_2(x)\rangle^0 - \langle y-f_1(x)\rangle^0) + (\langle x-x_2\rangle^0 - \langle x-x_1\rangle^0)(-f_2'(x)\langle y-f_2(x)\rangle^{-1} + f_1'(x)\langle y-f_1(x)\rangle^{-1}), \quad (8)$$

$$\frac{\partial \Lambda(x,y)}{\partial y} = (\langle x-x_2\rangle^0 - \langle x-x_1\rangle^0)(\langle y-f_2(x)\rangle^{-1} - \langle y-f_1(x)\rangle^{-1}). \quad (9)$$

Equations (7)–(9) allow for concise modelling of the transducer distribution and the piezoelectric differential operator. The second derivatives are given in Sullivan *et al*. [5]. The use of generalized functions for the mathematical representation of the distribution and the operator allows the modal coefficients to be calculated analytically. These tools will be used in the following section to examine the effects of transducer shading.

3. TWO-DIMENSIONAL TRANSDUCER DESIGN

3.1. CONTINUOUS, LINEARLY-WEIGHTED DISTRIBUTION

Using the mathematics developed in the preceding section, it is possible to analytically represent transducer distributions and to calculate their modal coefficients when applied to thin plates. Referring to the two-dimensional shaded distribution described in section 2.1 and pictured in Figure 5, the spatial distribution for this continuous, linearly-weighted shading can be represented by

$$\Lambda(x,y) = (\langle x\rangle^0 - (1/a)\langle x\rangle^1 + (1/a)\langle x-a\rangle^1)(\langle y\rangle^0 - (1/b)\langle y\rangle^1 + (1/b)\langle y-b\rangle^1). \quad (10)$$

The linear weighting in two dimensions is described by the "ramp" generalized functions. The differential operator result for this distribution is given by

$$L[\Lambda(x,y)] = e_{31}^0(\langle x\rangle^{-2} - (1/a)\langle x\rangle^{-1} + (1/a)\langle x-a\rangle^{-1})(\langle y\rangle^0 - (1/b)\langle y\rangle^1 + (1/b)\langle y-b\rangle^1) + e_{32}^0(\langle x\rangle^0 - (1/a)\langle x\rangle^1 + (1/a)\langle x-a\rangle^1)(\langle y\rangle^{-2} - (1/b)\langle y\rangle^{-1} + (1/b)\langle y-b\rangle^{-1}). \quad (11)$$

This result includes weighted delta functions along the boundaries. For a simply-supported plate, these will vanish due to the pinned boundary conditions. Thus,

the result given in equation (11) can be simplified by dropping these terms and pulling out the linear weighting from the generalized functions to yield,

$$L[\Lambda(x, y)] = e_{31}^0(1 - (y/b))\langle x\rangle^{-2}(\langle y\rangle^0 - \langle y - b\rangle^0) + e_{32}^0(1 - (x/a))\langle y\rangle^{-2}(\langle x\rangle^0 - \langle x - a\rangle^0). \quad (12)$$

This equation includes the linearly-weighted doublet functions along the sides $x = 0$ and $y = 0$, shown in Figure 6. The nth modal coefficient is calculated by substituting equations (6) and (12) into equation (5) and integrating in x and y to give

$$b_n = e_{31}^0(r/q)(b/a) + e_{32}^0(q/r)(a/b). \quad (13)$$

The integration of the transducer distribution with the modal shape results in the weighted slope of the modal shape being sifted out along the two sides and then integrated over the length of the sides. As can be seen from equation (13), the modal coefficient derived for this shaded transducer will be non-zero for all r and q. Thus, both controllability and observability are guaranteed whether the transducer is used as an actuator or a sensor.

This shading would prove useful for controlling vibrations in simply-supported plates because of its all-mode actuation and sensing properties. Unfortunately, it is difficult to effect this shading directly. The methods described in section 2.2. are very difficult to manufacture. One method, however, that *can* be implemented is an approximation of the shading using a sum of gain-weighted transducer sections. Trying to approximate a two-dimensional shading such as that shown in Figure 5 using a two-dimensional array of rectangular sections would be difficult because of the large number of sections that would be needed. The number of transducer sections needed to provide a good approximation could be reduced if the transducer shape was used to aid in the approximation.

3.2. TRANSDUCER SHAPING: TRIANGULAR DISTRIBUTION

Triangular-shaped transducers can be used to capture part of the linear ramp function present in the continuous shading. As a first step at approximating the continuous, linearly-weighted transducer distribution shown in Figure 5, consider the triangular distribution shown in Figure 8.

This distribution, like the linearly-weighted shading, is at a maximum at the origin and decreases to zero along both x and y through the decrease of surface area covered by the transducer. Using two-dimensional distributions with composite functions in the arguments, the transducer distribution is represented by

$$\Lambda(x, y) = (\langle x\rangle^0 - \langle x - a\rangle^0)(\langle y\rangle^0 - \langle y + (b/a)x - b\rangle^0). \quad (14)$$

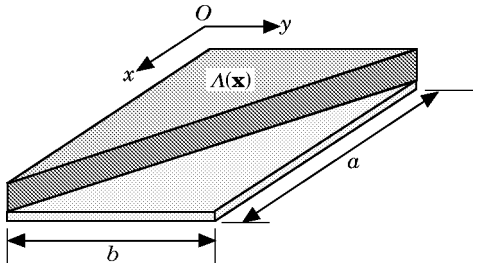

Figure 8. Triangular transducer distribution.

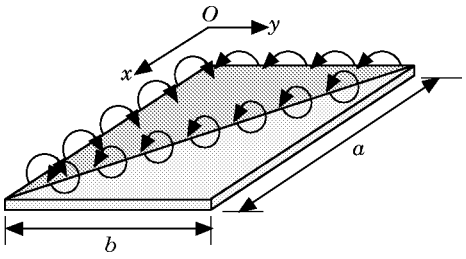

Figure 9. Resultant control input/sensed output for triangular transducer distribution.

The differential operator result is given by

$$L[\Lambda(x,y)] = e_{31}^0(\langle x\rangle^{-2} - \langle x-a\rangle^{-2})(\langle y\rangle^0 - \langle y+(b/a)x-b\rangle^0) + (\langle x\rangle^0 - \langle x-a\rangle^0)[e_{32}^0\langle y\rangle^{-2} - ((b^2/a^2)e_{31}^0 + e_{32}^0)\langle y+(b/a)x-b\rangle^{-2}] - 2(b/a)e_{31}^0(\langle x\rangle^{-1} - \langle x-a\rangle^{-1})(\langle y+(b/a)x-b\rangle^{-1}), \tag{15}$$

and is shown in Figure 9. Because the weighting is uniform within the shape boundary, the operator results in uniform doublet functions along the transducer boundary. Delta functions were also obtained at the vertices, but these were eliminated due to the simply-supported boundary conditions for the plate under consideration. The modal coefficients that arise from this distribution will be the sum of line integrals of the modal slope along boundaries $x = 0$, $y = 0$ and along the hypotenuse of the triangle. The modal coefficients that result from the application of this distribution to a simply-supported plate are given by,

$$b_n = e_{31}^0(r/q)(b/a)[(-1)^q - 1] + e_{32}^0(q/r)(a/b)[(-1)^r - 1] + \frac{q\pi}{b}\left(\frac{b^2}{a^2}e_{31}^0 + e_{32}^0\right)(-1)^q \int_0^a \sin(r\pi x/a)\cos(q\pi x/a)\,\mathrm{d}x. \tag{16}$$

The first two terms show the result of the doublet functions acting along sides $x = 0$ and $y = 0$. Along $x = 0$, whenever q is even, the line integral along this side is zero. The result of the doublet functions acting along the hypotenuse is shown in the last term of equation (16). The calculation of this integral depends upon whether $r = q$:

$$\int_0^a \sin(r\pi x/a)\cos(q\pi x/a)\,\mathrm{d}x = 0, \qquad (r = q), \tag{17}$$

$$\int_0^a \sin(r\pi x/a)\cos(q\pi x/a)\,\mathrm{d}x = -(a/2\pi)\{(1/(r-q))[(-1)^{r-q} - 1] + (1/(r+q))[(-1)^{r+q} - 1]\}, \qquad (r \neq q). \tag{18}$$

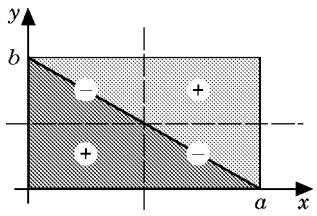

Figure 10. Triangular distribution shown with 2,2 mode (— — nodal lines).

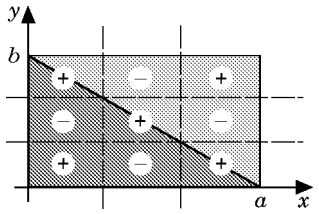

Figure 11. Triangular distribution shown with 3,3 mode (— — nodal lines).

Whenever $r = q$, the line integral along the hypotenuse will be zero. When $r = q =$ even, as in Figure 10, the line integrals along $x = 0$ and $y = 0$ are also zero so the modal coefficient sums to zero. However, when $r = q =$ odd, as shown in Figure 11, the line integrals along $x = 0$ and $y = 0$ are both non-zero so the modal coefficient for this case is non-zero. The reason for the zero line integral along the hypotenuse, however, can be seen by examining both Figures 10 and 11 and noting that each " + " or " − " rectangular section acts like a smaller plate in the 1–1 mode. Whenever the transducer hypotenuse extends from one corner of the " + " or " − " section to another, the line integral along this section will be zero. The distribution sifts out the slope of the mode shape along the hypotenuse and legs of the triangle. The contribution of the hypotenuse to the modal coefficient will be zero whenever the slope along the hypotenuse integrates to zero over the length of the plate.

For r and q not equal and both odd, the line integrals along all sides will be non-zero. For r and q not equal and either r or q is even, as shown in Figure 12, the line integral along one of the sides of the plate will be zero but the integral along the hypotenuse will be non-zero. For r and q not equal, but both even, all of the line integrals, and hence the modal coefficient, will be zero. This can be seen in Figure 13. The reason for the zero line integral along the hypotenuse in this case is due to the way the hypotenuse cuts through the sections between the nodal lines. The line integrals from the two " − " sections intersected by the hypotenuse sum to zero as do the line integrals from the two " + " sections that are intersected.

This shaped transducer distribution can control or sense the odd–odd, odd–even, and even–odd modes of a simply supported plate. It cannot, however, control or sense any of the even–even modes of a simply-supported plate. This makes the distribution very useful for the acoustic radiation attenuation problem because the odd–odd modes are the most efficient acoustic radiators while the odd–even and even–odd modes radiate sound to a lesser extent, and the even–even modes do not contribute significantly to the radiated sound field [3]. This transducer can be used to form a colocated sensor/actuator pair which will only sense and do work on those modes which have a significant contribution to the radiated sound field.

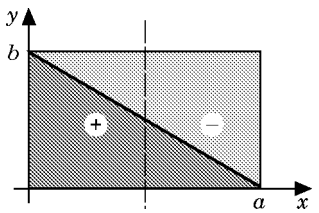

Figure 12. Triangular distribution shown with 2,1 mode (— — nodal lines).

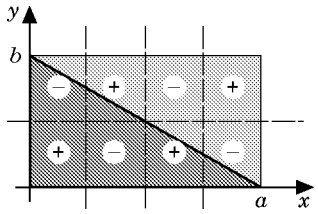

Figure 13. Triangular distribution shown with 4,2 mode (— — nodal lines).

3.3. GAIN-WEIGHTED APPROXIMATION TO LINEARLY-WEIGHTED SHADING

If global vibration suppression of a simply supported plate is desired, the triangular distribution will not suffice. The previous analysis shows that using shape to approximate shading in two-dimensions is more difficult than using it to approximate shading for beams. The two-dimensional linear shading is necessary to provide global controllability and observability. It is possible to approximate this shading for a large number of modes using an array of gain-weighted, shaped transducers as shown in Figure 14. This distribution is a sum of smaller distributions which are gain weighted. The distribution linearly decreases in the x direction due to the triangular shaping and decreases by steps in the y direction because of the gain-weighting.

The differential operator result of this distribution is shown in Figure 15. Doublet functions are obtained along the boundaries of the transducer sections but their magnitudes vary from section to section depending upon the gain that is given to each section. In the figure, for clarity, the doublet functions along the sides are represented by a resultant doublet function acting on the middle of the side.

The modal coefficients for the linearly-weighted shading are given by equation (13). To determine the best approximation, the modal coefficients of the gain-weighted array of transducer sections can be calculated and compared to those of the linearly-weighted shading.

The transducer distribution, $\Lambda(\mathbf{x})$, of a gain weighted array is the sum of the individual transducer distributions of the sections (with the gains of the sections included in each distribution):

$$\Lambda(\mathbf{x}) = \sum_{s=1}^{S} \Lambda_s(\mathbf{x}), \tag{19}$$

where S is the total number of sections used in the approximation. The nth modal coefficient for the transducer distribution is given by the sum of the nth modal coefficients calculated for each section,

$$b_n = \sum_{s=1}^{S} \int_D \varphi_n(\mathbf{x}) L[\Lambda_s(\mathbf{x})]\, \mathrm{d}\mathbf{x} = \sum_{s=1}^{S} b_{n,s}. \tag{20}$$

The geometry of a triangular section to be used in the array is shown in Figure 16. Each section is an isosceles triangle with a length equal to the total length of the plate, a. Note that the use of an asymmetric triangle section would yield even better controllability and observability results. The section's spatial distribution is given by

$$\Lambda_s(x, y) = g_s(\langle x\rangle^0 - \langle x - a\rangle^0)(\langle y - m_s x - v_s^l\rangle^0 - \langle y + m_s x - v_s^h\rangle^0), \tag{21}$$

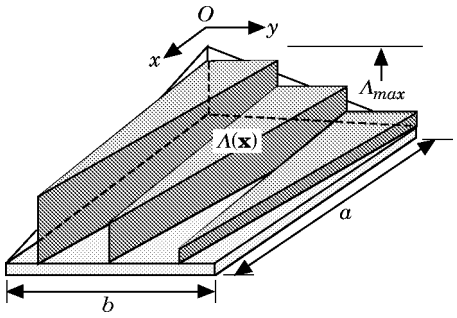

Figure 14. Approximation of two-dimensional linear shading.

where g_s is the gain assigned to the section,

$$g_s = -((v_s^l + v_s^h)/2)\,(\Lambda_{\max}/b) + \Lambda_{\max}. \tag{22}$$

This section gain is chosen such that the midpoint of the transducer section intersects a line defining the ideal gain over the plate width as shown in Figure 17.

Again, the differential operator acting on this distribution will produce doublet functions lining the boundary,

$$\begin{aligned} L[\Lambda(x,y)] = {} & e_{31}^0(\langle x\rangle^{-2} - \langle x-a\rangle^{-2})(\langle y - m_s x - v_s^l\rangle^0 - \langle y + m_s x - v_s^h\rangle^0) \\ & + (m_s^2 e_{31}^0 + e_{32}^0)(\langle x\rangle^0 - \langle x-a\rangle^0)(\langle y - m_s x - v_s^l\rangle^{-2} - \langle y + m_s x - v_s^h\rangle^{-2}) \\ & - 2m_s e_{31}^0(\langle x\rangle^{-1} - \langle x-a\rangle^{-1})(\langle y - m_s x - v_s^l\rangle^{-1} + \langle y + m_s x - v_s^h\rangle^{-1}). \end{aligned} \tag{23}$$

Their magnitude is uniform along each side because the gain of the section is constant over its spatial extent. Delta functions are also obtained at the vertices, but these disappear due to the pinned boundary conditions.

The modal coefficient for this section is

$$\begin{aligned} b_{n,s} = g_s & \left[\cos\left(\frac{q\pi v_s^h}{b}\right) - \cos\left(\frac{q\pi v_s^l}{b}\right)\right] \times \left\{e_{31}^0(r/q)(b/a) + \tfrac{1}{2}(m_s^2 e_{31}^0 + e_{32}^0)\right. \\ & \left. \times \left(\frac{q\pi}{b}\right)\left[\left(\frac{r\pi}{a} + \frac{q\pi m_s}{b}\right)^{-1} + \left(\frac{r\pi}{a} - \frac{q\pi m_s}{b}\right)^{-1}\right]\right\}. \end{aligned} \tag{24}$$

The modal coefficient for the section will equal zero whenever a nodal line in x bisects the triangle. In this case, an example of which is shown in Figure 18 for $q = 2$ and $S = 1$, the midpoint between v_s^h and v_s^l is equal to bj/q where j is any integer. This relationship causes the first two cosine terms on the right side of equation (24) to be equivalent and their difference to thus be equal to zero. So, when different transducer sections of equal widths

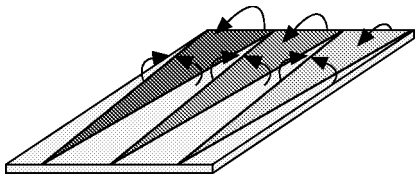

Figure 15. Resultant control input/sensed output of linear two-dimensional shading approximation.

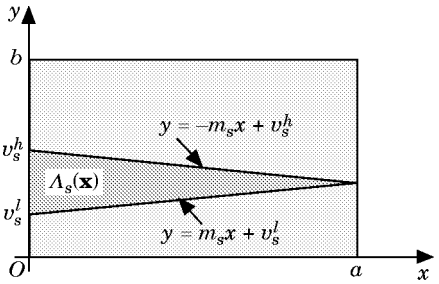

Figure 16. Triangular transducer section geometry.

are added together, even with different gains, as shown in Figure 19, cancellation occurs when $q = 2S$ for all r. Because of this cancellation, one must employ unequal segment widths to change the inherent symmetry.

As an aside, the last term in equation (24) appears to go to infinity when $m_s = b/(2Sa)$ and $q = 2Sr$. The slope condition occurs whenever the sections have equal widths or whenever there is only one section. This can be seen from Figure 18. In this case, $m_s = b/(2a)$ and this term appears to go to infinity. However, using L'Hospital's rule, it can be shown that, when $q = 2Sr$ and the slope approaches $b/(2Sa)$, this term is well-behaved and goes to zero.

The benefit of using unequal widths in the approximation becomes apparent when the spatial Fourier transform is applied to the problem. It is possible to separate the problem into x and y components because of the plate's simply-supported boundary conditions. Examination of the y component will help determine the controllability/observability characteristics of the transducer distribution because the step approximation occurs along this direction. Imagine taking a slice of the transducer distribution along the line $x = 0$. The transducer distribution will look like a staircase function in this case. One will be comparing this function to that shown as the ideal function, the gain of the linear two-dimensional distribution, shown in Figure 17. Using this transform method involves less analysis than calculating the modal coefficients for each transducer distribution as a whole. Thus, it provides a useful tool for the evaluation of the controllability/observability properties of candidate distributions. The Fourier transform of the PVDF operator acting on the y component of a transducer distribution, $L[\Lambda(y)]$ is given by,

$$h(k) = \frac{1}{\sqrt{2\pi}} \int_0^b L[\Lambda(y)] e^{iky} \, \mathrm{d}y, \tag{25}$$

where the limits of integration are reduced from $(-\infty, +\infty)$ to [0, b] because the transducer distribution is bounded by the width of the plate, b. The spatial variable k is the wavenumber component in the y direction.

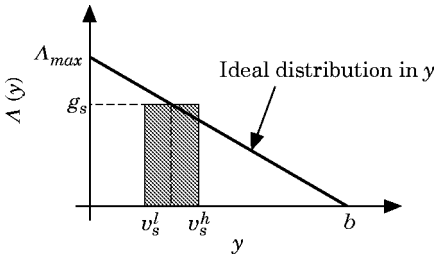

Figure 17. Transducer section gain weighting.

The magnitude of the imaginary part of the transform is given by

$$h_{imag}(k) = \left| \int_0^b L[\Lambda, (y)] \sin(ky)\, \mathrm{d}y \right|. \tag{26}$$

This is equivalent to the expression for the y component of the nth modal coefficient when $k = q\pi/b$. Examination of this part of the transform is relevant to assessing the impact of the distribution on the plate mode shapes. Simply looking at the entire Fourier transform would not be useful because plate modal information would not be taken into account. Since the imaginary part of the transform is a continuous version over k of the y-component of the modal coefficient equation, the information obtained can be used to determine controllability and observability characteristics of the transducer acting on the simply-supported plate.

First, consider the ideal distribution in y shown in Figure 17. This distribution can be represented by

$$\Lambda(y) = \langle y \rangle^0 - (1/b)[\langle y \rangle^1 - \langle y - b \rangle^1]. \tag{27}$$

The PVDF operator acting on this distribution is given by

$$L[\Lambda(y)] = \langle y \rangle^{-2}. \tag{28}$$

The point forces have been eliminated due to the boundary conditions leaving only a positive moment at $y = 0$. The Fourier transform for this case is

$$h(k) = -\mathrm{i}k. \tag{29}$$

Since the transform is purely imaginary, the magnitude of the imaginary component is simply k and is thus non-zero for all k. Thus this ideal distribution has all-mode controllability and observability.

Now consider the case of an individual transducer section used in an approximation of the ideal distribution. The y component of the transducer distribution given in equation (21) along the line $x = 0$ is given by

$$\Lambda_s(y) = (\langle y - v_s^l \rangle^0 - \langle y - v_s^h \rangle^0). \tag{30}$$

The PVDF operator acting on this individual section distribution is

$$L[\Lambda_s(y)] = g_s(\langle y - v_s^l \rangle^{-2} - \langle y - v_s^h \rangle^{-2}). \tag{31}$$

This result shows doublet functions (or moments) acting in opposition at the ends of the section. The Fourier transform of (31) is

$$h(k) = -\mathrm{i}kg_s(e^{\mathrm{i}kv_s^l} - e^{\mathrm{i}kv_s^h}). \tag{32}$$

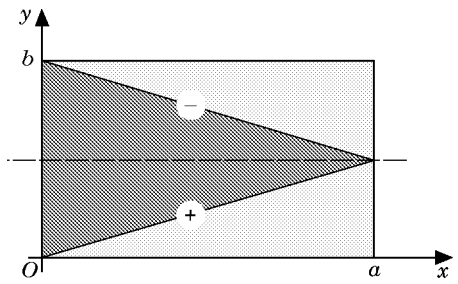

Figure 18. Transducer section shown with 1,2 mode (— — nodal line).

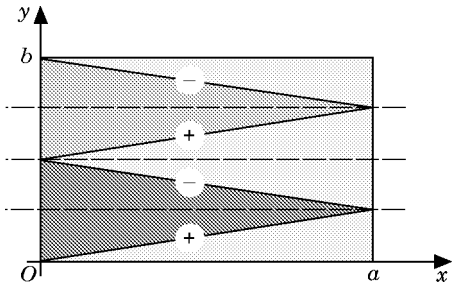

Figure 19. Equal width transducer sections shown with 1,4 mode (— — nodal line).

The magnitude of the imaginary component is

$$h_{imag}(k) = |kg_s[\cos(kv_s^l) - \cos(kv_s^h)]|. \tag{33}$$

From this equation, it is evident that whenever a nodal point occurs at the midpoint of the transducer section, no matter how large or small the section, a zero result will be obtained for the imaginary component of the Fourier transform. The opposing doublet moments produced by the transducer distribution will not be able to do any work or sense any angular displacement because of the symmetry involved. Thus, the particular mode for which this occurs will not be controllable or observable.

The following plots illustrate this point and also demonstrate the benefit of using sections with unequal widths. The first two plots, shown in Figure 20, show an approximation to the ideal distribution using only two sections of equal width and the imaginary part of the Fourier transform of such a distribution. The even modes, occurring at $k = 2\pi/b, 4\pi/b, 6\pi/b, \ldots$, are marked with an "$x$" on the wavenumber transform plot. The transform of the ideal distribution is shown with a dotted line while the transform of the approximation is shown with a solid line. The zeros of the approximation occur

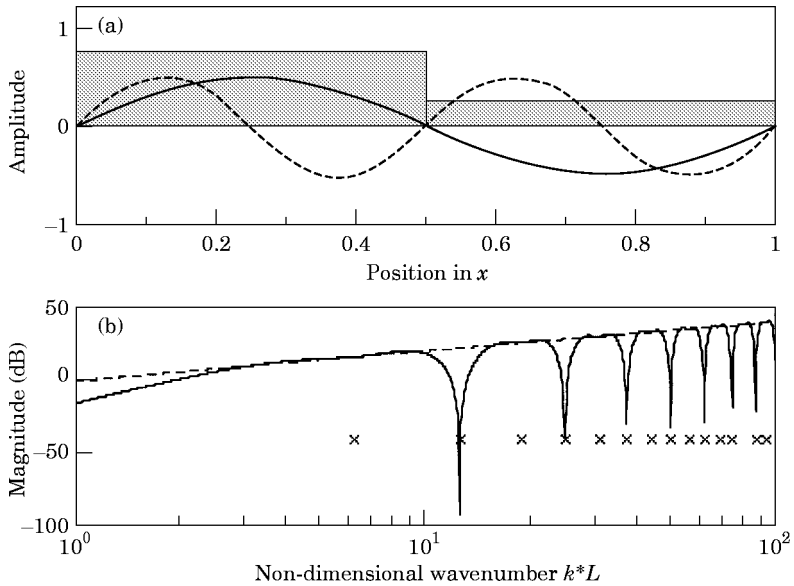

Figure 20. (a) Equal width section approximation shown as shaded boxes with overlay of second mode (——) and fourth mode (- - - -), (b) wavenumber sine transform of equal width section approximation (——) and of ideal distribution (- - - -) shown with even mode wavenumbers (×).

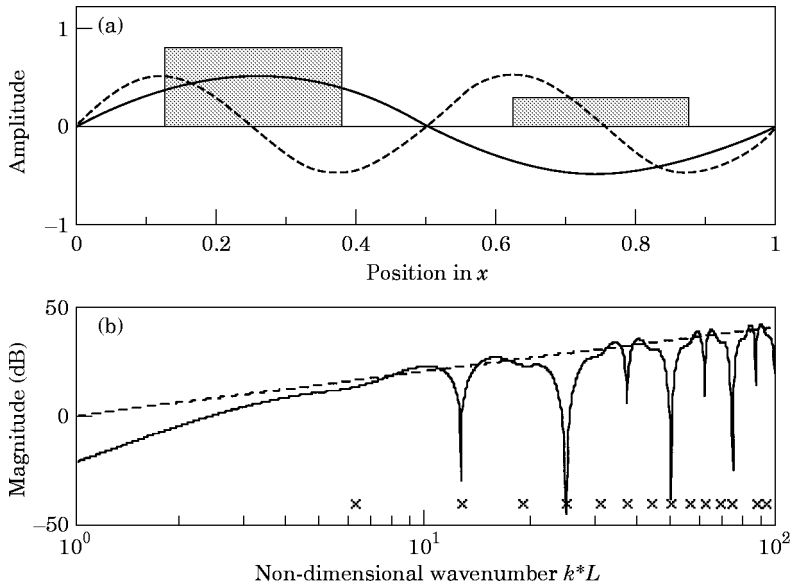

Figure 21. (a) Reduced width section approximation shown as shaded boxes with overlay of second mode (——) and fourth mode (- - - -), (b) wavenumber sine transform of reduced width section approximation (——) and of ideal distribution (- - - -) shown with even mode wavenumbers (×).

at every other even mode beginning with $k = 4\pi/b$. Thus, this approximation to the ideal distribution can control/observe the first three modes of the plate, $k = \pi/b$, $2\pi/b$, and $3\pi/b$ before reaching a zero for the fourth mode. The mode shapes of the second and fourth mode are shown in the top plot. Since the transducer sections have different gains, the second mode is controllable. However, the fourth mode is not controllable because it has nodal points which occur in the middle of each transducer section.

The next two plots, pictured in Figure 21, show that the same results are obtained when the width of the sections is reduced, but the midpoints are kept at the same location. In this case, the widths were reduced by the same amount, but the result would be the same even if they were of unequal width. Since the midpoints of each section are the same, they will still lack the asymmetry needed to control or observe the fourth mode.

The final plots in Figure 22 demonstrate improved controllability/observability characteristics using transducer sections with different widths and midpoints located in different points. The result is that the first five modes are now controllable/observable using only two transducer sections. On the transducer section plot, the solid line shows the mode shape of the fourth mode and the dashed line shows the mode shape of the sixth mode. It is not until the sixth mode, $k = 6\pi/b$, that nodal points will occur at the midpoints of the transducer sections.

The wavenumber transform analysis demonstrates that one can allow the section widths to be degrees of freedom in an optimization problem that seeks to miminize the difference between the ideal distribution and the approximation. The analytical method is also a useful tool for understanding the physics of the transducer distribution's interaction with the plate mode shapes.

The design process can be reduced to a minimization problem with the following quadratic objective function:

$$J = \sum_{n=1}^{N} (b_{n,ideal} - b_{n,approx}(\boldsymbol{\alpha}))^2 = \| \mathbf{b}_{ideal} - \mathbf{b}_{approx}(\boldsymbol{\alpha}) \|^2, \tag{34}$$

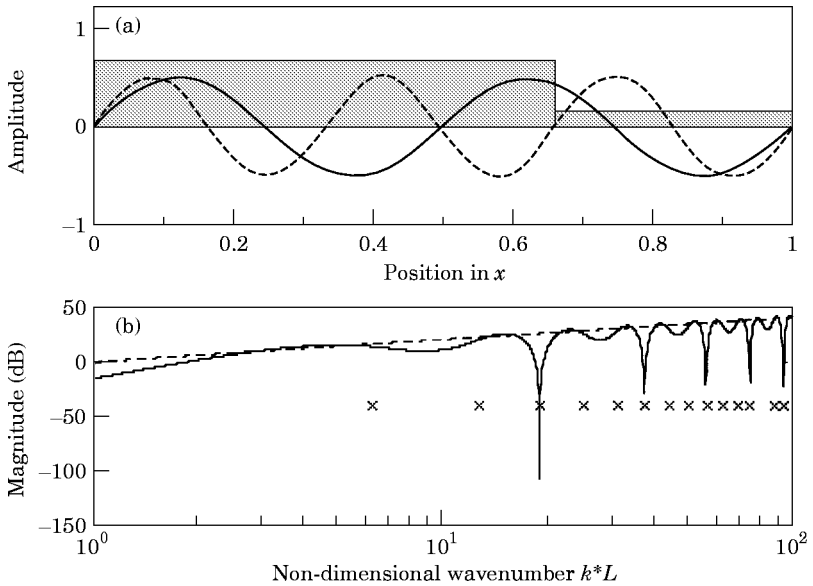

Figure 22. (a) Unequal width section approximation shown as shaded boxes with overlay of fourth mode (——) and sixth mode (- - - -), (b) wavenumber sine transform of unequal width section approximation (——) and of ideal distribution (- - - -) shown with even mode wavenumbers (×).

where the $\mathbf{b}_{ideal}$ vector corresponds to the modal coefficients of the continuous, linearly-weighted shading and the $\mathbf{b}_{approx}$ vector corresponds to the modal coefficients of the gain-weighted approximation. The vector $\boldsymbol{\alpha}$ is composed of the section widths, α_s, of the first $S-1$ sections. These are the independent variables in the minimization problem. The width of the last section is a dependent variable because it is equivalent to the difference between the width of the plate, b, and the sum of the first $S-1$ sections. Overlap between sections is not allowed because this would complicate the optimization process and there is no apparent benefit from doing this. Gaps between sections are not allowed because the overall actuator authority or sensor sensitivity would be decreased. The number of sections, S, and the number of modes, N, used in the optimization problem are both parameters to be determined prior to minimization.

The number of sections is dependent upon the width of the plate, b, because too large a number for a given plate width would yield section widths too small to be easily fabricated or positioned on the plate. The number of modes, N, used in the optimization problem should be large enough to include all modes within the control bandwidth. As N becomes very large, however, it will become more difficult to obtain a good approximation because more degrees of freedom are needed for the optimization. An important consideration becomes the values of the modal coefficients outside the desired bandwidth. This is because, in a real system, noise and phase lags can cause instability in high frequency modes with strong modal coupling. When a global controller such as velocity feedback is used, these modes can be destabilized. Thus, it is important to perform the optimization over a certain number of modes N and then check the values of the modal coefficients for the higher order modes.

All of the constraints for the problem relate to the geometry. The sections are chosen to be isosceles triangles with length equal to the length of the plate. Each width must be larger than a certain minimum width, α_{min}, and this width must be greater than zero. All

sections must touch on the $x = 0$ side of the plate. Also, the total width of the sections cannot exceed the width of the plate.

The objective function was written as a MATLAB function to be minimized by the "fmins" function included in the MATLAB toolbox. This function uses an unconstrained non-linear optimization scheme to find the minimum of a function of several variables. Most of the geometric constraints for this problem were written into the definition of the objective function. Two constraints could not be included in this way: the minimum width constraint and the total width maximum. They were included by heavily penalizing the objective function when they were violated.

This research was concerned with matching an implementable distribution with an ideal distribution that had known controllability and observability properties. However, the analysis and optimization techniques can be applied to a more general case. One may define a modal coefficient profile that has a desired shape in the wavenumber domain. For example, if one is using a global controller such as velocity feedback, a desired profile would include roll-off after a defined bandwidth. In this manner, the transducer would not couple strongly into those modes for which the phase lags in the system summed to greater than 90 degrees, thus facilitating a higher velocity feedback gain. This would allow spatial compensation using distributed transducers to compensate for temporal phase lags in a hardware implementation.

The ideal distribution would then be defined by the desired modal coefficient profile, $\mathbf{b}_{ideal}$, and the optimization process would attempt to match some unknown transducer distribution to this profile. Since the geometry of the ideal distribution would be unknown, the geometry of the approximation could be changed to allow more degrees of freedom. For example, the plate could be divided up into a grid with a rectangular transducer section assumed to be covering each grid section. The gain of each transducer section would be allowed to vary between a minimum and maximum value. The gains of each section would then become degrees of freedom used in the optimization problem. The optimization process would then be exercised and the results examined to see if an inherent geometry and symmetry exists. Then, suitable transducer shapes and gain-weighting could be applied to the problem so that the number of transducer sections could be reduced. The optimization process could take place again using a reduced number of degrees of freedom. In this manner, it would be possible to achieve a desired modal coefficient profile using a finite number of shaped, gain-weighted transducers.

4. DESIGN EXAMPLE

The design process for the approximation outlined in section 3.3. was applied to a sample plate with $a = 0{\cdot}671$ m, $b = 0{\cdot}469$ m. Uniaxial PVDF film was used, with $d^0_{3'1'} = 23 \times 10^{-12}$ C/N and $d^0_{3'2'} = 3 \times 10^{-12}$ C/N, $Y_p = 2 \times 10^9$ N/m^2, and $v_p = 1/3$. The number of modes chosen over which to optimize was 10 and the number of sections chosen was 5. The initial estimate for α was chosen such that all of the sections widths were equal. The minimum width was 5 cm.

The minimization routine converged and the result was checked by starting from several different initial estimates for the width vector. This was done to see if the minimum obtained was local or "global" for the allowable range of widths. The resulting widths are $\alpha = [8{\cdot}2 \;\; 6{\cdot}4 \;\; 11{\cdot}0 \;\; 10{\cdot}4]$ cm. The resulting modal coefficients are compared to the linearly-weighted ideal shading in Figure 23. The modal coefficients have been normalized such that the largest has unit amplitude. The modal coefficients obtained for $N < 10$ were in excelllent agreement with those obtained for the linearly-weighted shading. The percentage error is less than 1% for those with $n < 10$. However, even for those modes

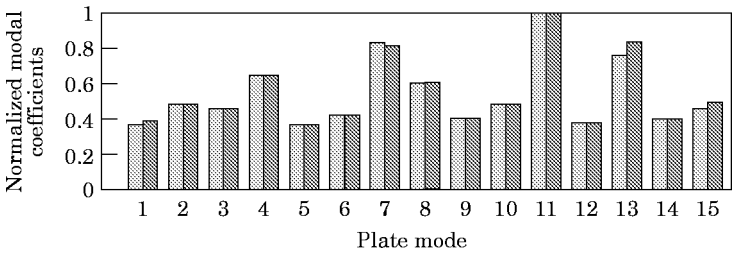

Figure 23. Normalized modal coefficients of ideal (linear) shading and approximation: ▤, ideal; ▧, approximated.

just outside of the control bandwidth, the percentage error is less than 10%. It is interesting to note that the error was greatest for modes 13 and 15. For the given plate, these mode numbers correspond to the 1,4 and 2,4 modes. These are the only two modes shown for which $q = 4$. The errors associated with these modes are large because they are the most difficult to match due to the discrete gain-weighting approximation in the y direction.

The optimization results show that it is possible to obtain a close approximation to a desired continuous two-dimensional shading using gain-weighted, shaped transducers. This procedure can be extended to problems where it is desired to have the modal coefficients fit a predetermined profile over mode number. One can envision such a profile as having relatively equal modal coefficients within a certain bandwidth with those coefficients outside of the bandwidth decreasing with increasing mode number. In this manner, the gain of a feedback controller could be increased to control modes within the bandwidth without destabilizing the modes outside of the bandwidth. This would allow spatial compensation using distributed transducers to compensate for temporal phase lags in a hardware implementation. Or, one might wish to target a small group of modes within a certain frequency range.

5. CONCLUSIONS

The motivation for two-dimensional transducer shading was presented and various methods for achieving shading were considered for the active control of thin plates. Two-dimensional transducer shaping was shown to be a useful design tool for the control problem. It was also shown that transducer shaping can be combined with gain-weighting to provide close approximation of continuously shaded transducer distributions. The analysis was applied to two specific examples. One utilizes two-dimensional transducer shaping alone to establish controllability and observability over all but the even–even modes in a simply-supported plate. This transducer distribution is a very practical solution for the acoustic radiation attenuation problem. The second distribution is a superposition of gain-weighted, shaped transducer sections providing a good approximation to a continuous two-dimensional shaded transducer distribution. This distribution provides "all-mode" controllability and observability over a large bandwidth and is therefore useful for global vibration suppression in plates. An optimization method used to fit the approximation to the continuous transducer distribution over a specified number of modal coefficients was described.

ACKNOWLEDGMENTS

This research was supported by the Charles Stark Draper Laboratory, Inc., under IR&D Project # 466. The preparation of this paper for journal publication was supported by

the Mathematics and Geosciences Directorate of the Air Force Office of Scientific Research (AFOSR). The authors would also like to thank Dr. John Meyer for his valuable suggestions.

REFERENCES

1. C.-K. Lee and F. C. Moon 1989 *Journal of the Acoustical Society of America* **85**, 2432–2439. Laminated piezopolymer plates for torsion and bending sensors and actuators.
2. S. E. Burke and J. E. Hubbard Jr. 1991 *Journal of the Acoustical Society of America* **90**, 937–944. Distributed transducer vibration control of thin plates.
3. R. L. Clark and C. R. Fuller 1991 *Journal of Intelligent Material Systems and Structures* **2**, 431–452. Control of sound radiation with adaptive structures.
4. S. E. Burke and J. E. Hubbard Jr. 1990 *Journal of Dynamic Systems, Measurement, and Control* **112**, 565–573. Spatial filtering concepts in distributed parameter control.
5. J. M. Sullivan, J. E. Hubbard Jr. and S. E. Burke 1996 *Journal of the Acoustical Society of America* **99**, 2965–2974. Modelling approach for two-dimensional distributed transducers of arbitrary spatial distribution.
6. S. E. Burke and J. E. Hubbard Jr. 1988 *Automatica* **24**, 619–627. Distributed actuator control design for flexible beams.
7. S. E. Miller and J. E. Hubbard Jr., 1987 *Proceedings of the 6th VPI&SU/AIAA Symposium on Dynamics and Control of Large Structures, Blacksburg, VA*, Observability of a Bernoulli–Euler beam using PVF_2 as a distributed sensor.
8. S. E. Burke and J. E. Hubbard Jr. 1987 *IEEE Control Systems Magazine* 25–30. Active vibration control of a simply supported beam using a spatially distributed actuator.
9. C. K. Lee and F. C. Moon 1990 *ASME Journal of Applied Mechanics*, **57** 434–441. Modal sensors/actuators.
10. C. K. Lee, W. W. Chiang and T. C. O'Sullivan 1989 *AIAA Paper*, 89–1390-*CP*, 2018–2026. Piezoelectric modal sensors and actuators achieving critical active damping on a cantilever plate.
11. C. K. Lee, W. W. Chiang and T. C. O'Sullivan 1990 *Journal of the Acoustical Society of America* **90**, 374–383. Piezoelectric modal sensor/actuator pairs for critical active damping vibration control.
12. D. W. Miller, S. A. Collins and S. P. Peltzman 1990 *AIAA Paper*, 90–1127-*CP*, 2283–2297. Development of spatially convolving sensors for structural control applications.
13. R. L. Clark and C. R. Fuller 1992 *Journal of the Acoustical Society of America* **91**, 3321–3329. Modal sensing of efficient acoustic radiators with PVDF distributed sensors in active structural acoustic approaches.
14. R. L. Clark, R. A. Burdisso and C. R. Fuller 1993 *Journal of Intelligent Material Systems and Structures* **4**, 354–365. Design approaches for shaping polyvinylidene fluoride sensors in active structural acoustic control.
15. S. E. Burke and R. L. Clark 1995 *Smart Structures and Materials* 1995: *Smart Structures and Integrated Systems*, Inderjit Chopra, Editor, Proc. SPIE 2443, 410–421. Transducer tolerance theory for structural control.
16. E. K. Dimitriadis, C. R. Fuller and C. A. Rogers 1989 *Proceedings of the Eighth Biennial Conference on Failure Prevention and Reliability, Montreal, Canada*, 223–233. Piezoelectric actuators for distributed noise and vibration excitation of thin plates.
17. P. W. Smith, Jr. and R. H. Lyon 1965 *Sound and Structural Vibration*. National Aeronautics and Space Administration, NASA CR-160.
18. S. E. Burke, J. E. Hubbard Jr and J. E. Meyer 1991 *Symposium on Intelligent Structural Systems, ASME Thirteenth Biennial Conference on Mechanical Vibration and Noise, Miami, FL*, Colocation: design constraints for distributed and discrete transducers.
19. S. H. Crandall 1972 *An Introduction to the Mechanics of Solids*. New York: McGraw-Hill.